Machine Copy for Proofreading, Vol. x, y–z, 2014

Torque Calculation in Interior Permanent Magnet Synchronous Machine Using Improved Lumped Parameter Models

Hooshang Mirahki* **and Mehdi Moallem**

Abstract—In this paper, we present improved Lumped-Parameter Models for simulation of a Interior Permanent Magnet Synchronous (IPMS) machine to calculate of PM flux linkage, and Q and D-axis inductances which can be used for torque calculation. These improved models include all details of flux barriers and air bridges of rotor and also the effect of saturation in central posts and stator core. To validate the accuracy of these models, results are compared with the Finite Element Method results for a presented IPMS machine.

1. INTRODUCTION

Interior Permanent Magnet Synchronous (IPMS) machines due to their high efficiency, power density, power factor and torque density are increasingly being used in various applications, such as variable speed drives, electrical vehicles, and other industrial drives [1, 2]. Compared with Surface Permanent Magnet (SPM) machines, interior permanent magnet synchronous machines have robust rotor construction, high reluctance torque, and high demagnetization withstand. Also they are suitable for electric vehicles application which require a wide constant power operating speed range [1, 3].

Since Finite Element Analysis is highly time consuming for machine design and optimization process [3], researchers have always been looking for analytical methods that could be used for the purpose of machine optimization. The existing methods such as Laplacian or quasi-Poissonian methods solve the field equations for surface permanent magnet machine [4] or inset permanent magnet machine directly and use the conformal mapping for taking the effects of slots into consideration [4, 5]. Anyhow, because of the leakage flux, saturation in different parts and the complicated structure of the interior permanent magnet synchronous machine, it is not possible to use these analytical methods for the modeling and optimization of IPMS machine [6, 7]. The Magnetic Equivalent Circuits (MEC) method that is used for calculation of no-load and full-load field in Inductions [8], switched reluctance [9], salient-pole synchronous [10], SPM [11] and IPMS machines [7] is not an appropriate approach for optimization purposes due to its complexity and modeling efforts. The saturating Lumped Parameter Model (LPM) is one of the most efficient methods for optimization of IPMS machines especially in high-load conditions [12, 13], since it can include machine complex geometry and saturation in stator and rotor cores [14]. Due to its fast and accurate results in calculating machine parameters, LPM could be used in optimization process that needs thousands of iterations for finding an optimal solution [15, 16].

In this paper, three different models of lumped parameter are used for calculation of average torque [6, 12]. First, a linear lumped parameter model is used for calculation of PM flux linkage [14, 17]. For simplicity, the reluctances of the rotor yoke and stator yoke could be ignored compared to the reluctance of the air gap, the level of saturation in iron bridges and central posts are assumed constant [18, 19]. Two other lumped parameter models could be used for calculation of D and Q-axes inductances. Since the effective air gap in D-axis is large [20] the reluctance of rotor yokes and stator yokes could be ignored for calculation of D-axis inductance and also the variation under different

Received 30 September 2014

* Corresponding author: Hooshang Mirahki (h.mirahki@ec.iut.ac.ir).
The authors are with Department of Electrical and Computer Engineering, Isfahan University of Technology, Isfahan, Iran.

loading condition has no effect in saturation level in iron bridges; therefore, iron bridge length is added to flux barrier length but central posts are modeled with variable reluctance. In these models Carter coefficient could be used for taking slot effect into consideration [2, 17]. Since candidate IPMS machine is three layer and has no skew in rotor; therefore, are neglected cross coupling from the D-axis magnets and stator excitation. The mechanism of cross coupling depends on particular geometry such as number of layers and rotor skew [21, 22].

In this paper, we have succeeded to calculate PM flux linkage, inductances of Q- and D-axis and also the average torque of a three layer IPMS machine accurately using specially designed LPM method consisting of the effects of saturation of D-axis and stator core with detailed model of flux barriers and central posts. The results of our method are in excellent agreement with these obtained by Finite Element Method (FEM).

Table 1. IPMS machine parameters.

Name	symbol	Quantity
Number of poles	N_p	12
Number of layers	k	3
Winding factor	K_{a1}	0.933
Stator and rotor core material	-	M-19
Core length	L	60 [mm]
Stator inner radius	R_{si}	109 [mm]
Rotor outer radius	R_{ro}	108.4 [mm]
Number of series turns per phase	N_a	24
Number of slots	Q_s	72
Remnant flux density	B_r	0.46 [T]
Magnet span layers	$\alpha_1, \alpha_2, \alpha_3$	8, 17.5, 26.2 [mech.degrees]
Central posts	w_c	1 [mm]
Magnet width	$h_{m1},\ h_{m2},\ h_{m3}$	2, 3, 4 [mm]
Flux barrier width	$d_1,\ d_2,\ d_3$	1, 2, 3 [mm]
Width of air bridges	$w_{b1},\ w_{b2},\ w_{b3}$	0.75, 1.5, 1 [mm]
Length of air gap	g	0.6 [mm]
Magnet length	$w_{m1},\ w_{m2},\ w_{m3}$	10.5, 22, 27 [mm]

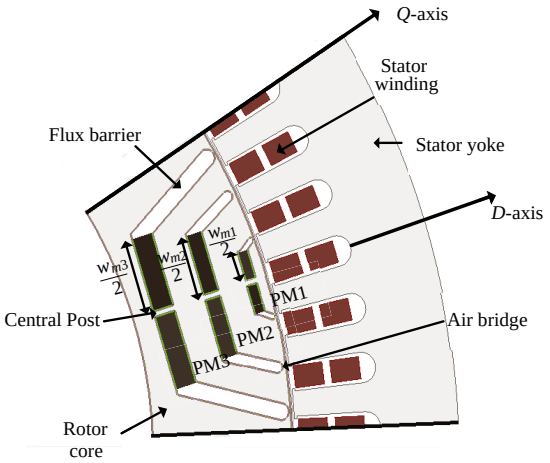

Figure 1. One pole of a 12-pole IPMS machine.

2. ELECTROMAGNETIC TORQUE

Figure 1 shows one pole of a 12-poles IPMS machine. In this configuration, each rotor pole contains three buried magnets. Machine basic parameters are given in Table 1.

The main aim of this paper is to obtain electromagnetic torque analytically. The following equation can be used to calculate the electromagnetic torque [1].

$$T_e = 3\left(\frac{N_p}{2}\right)\left(\lambda_{PM} I_q - (L_q - L_d)\, I_q I_d\right) \tag{1}$$

where N_p and λ_{PM} are the number of poles and PMs flux linkage, respectively. L_q, L_d, I_q and I_d are Q and D-axis inductances and current components, respectively. Although Equation (1) is typically used in linear lumped parameter model but it can be use for saturated LPM if the inductances are implicit functions of excitation [6]. Therefore, to obtain T_e, one needs to calculate PM flux linkage and Q and D-axis inductances by using the saturated lumped parameter model.

3. FLUX LINKAGE CALCULATION

The PM flux linkage, λ_{PM}, can be calculated using linear LPM. In this calculation assumptions of constant magnetic vector potential in the stator and rotor cores, fixed magnet remanence, and saturated constant flux density iron bridges are made [3]. The PM flux linkage, λ_{PM}, is calculated using Equation (2) and linear magnetic circuit model [1, 3].

$$\lambda_{PM} = \frac{4\sqrt{2} R_{ro} L N_a K_{a1} B_1}{N_p} \tag{2}$$

In this equation, B_1 and K_{a1} are fundamental air gap flux density and fundamental winding coefficient, respectively. Figure 2 shows three-layer IPMS machine designated as PM1, PM2 and PM3 with flux line. The calculated flux lines using Finite Element Analysis (FEA) clearly shows the locations of reluctances and flux sources. According to the paths of flux line obtained from FEA, lumped parameters model can be extracted as shown in Figure 3. In Figure 3, φ_{gk} for ($k = 1$ to 3) are air gap flux densities while the corresponding reluctances are $R_{gk} = \frac{g}{\mu_0 A_{gk}}$, where:

$$A_{gk} = \left(\alpha_{p(k)} - \alpha_{p(k-1)}\right) \frac{2\pi(R_{si} - \frac{g}{2})}{N_p} L, \quad \text{for} \quad (k = 2, 3) \tag{3}$$

$$A_{gk} = \alpha_{p(k)} \frac{2\pi(R_{si} - \frac{g}{2})}{N_p} L, \quad \text{for} \quad (k = 1) \tag{4}$$

where μ_0 is the permeability of air, and ($\alpha_{pk} = \frac{\alpha_k N_p}{2\pi}$) is the pole-arc to pole pitch ratio. $\varphi_{rk} = B_r w_{mk} L$, $\varphi_{mbk} = B_{satbk} L w_{bk}$, and $\varphi_{mbck} = B_{satck} L w_c$ are the flux sources, leakage fluxes of PMs through the

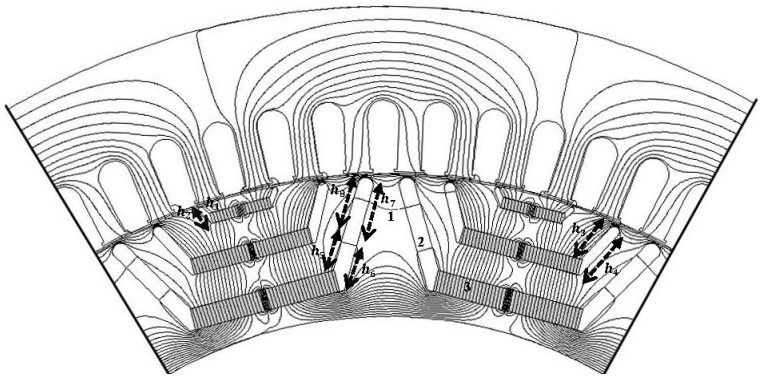

Figure 2. Flux lines for IPMS machine from FEM.

bridges, and leakage fluxes of PMs through the central posts, respectively. B_{satbk} and B_{satck} are the level of saturation in bridges and central posts, respectively. Since a part of flux lines of the third magnet flows through its own flux barrier and a part of it flows commonly through its own flux barrier and the flux barrier of the adjacent magnet, therefore for lumped parameter models, each flux barrier is divided into two reluctances. Hence, in Figure 2 the flux lines 1, 2, and 3 are corresponding to reluctances R_{kml1}, R_{1ml2} and R_{mok}, respectively.

$$R_{mok} = \frac{h_{mk}}{\mu_0 \mu_r w_{mk} L} \tag{5}$$

$$R_{kml1} = \frac{2h_{mk}}{\mu_0 L(h_n + h_{n+1})} \quad (k=1,\ n=1), \quad (k=2,\ n=3), \quad (k=3,\ n=5) \tag{6}$$

$$R_{3ml2} = \frac{4d_3}{\mu_0 L(h_7 + h_8)} \tag{7}$$

where h_n is the length of flux barrier. Since, there is no saturation in stator and rotor yokes, therefore R_{s1}, R_{s2}, R_{s3}, and R_r can be neglected in Figure 3(a) as compared with R_{gk}. Therefore, Figure 3(a) can

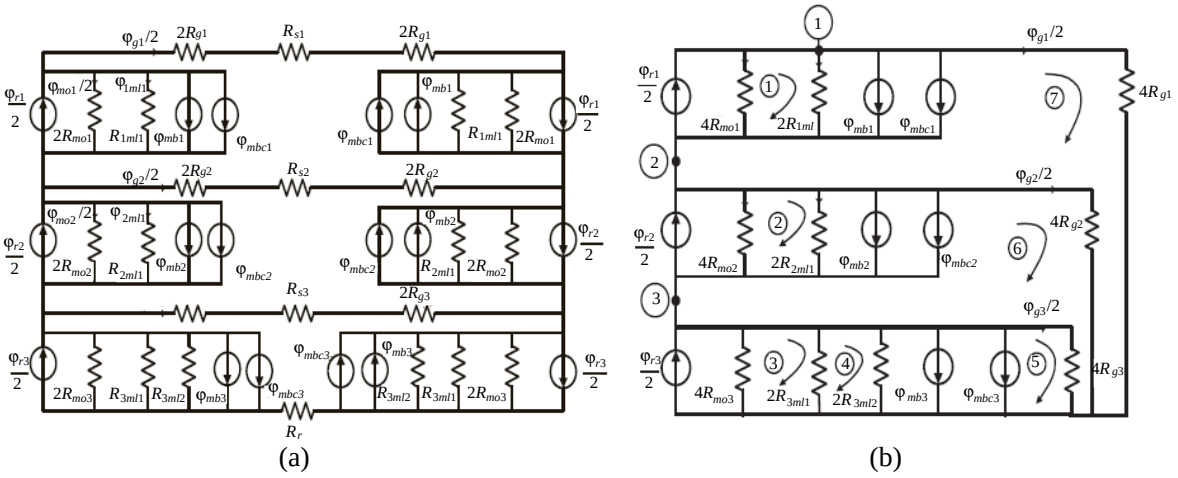

Figure 3. Lumped parameter model. (a) Lumped circuit model of IPMS. (b) Simplified lumped circuit model.

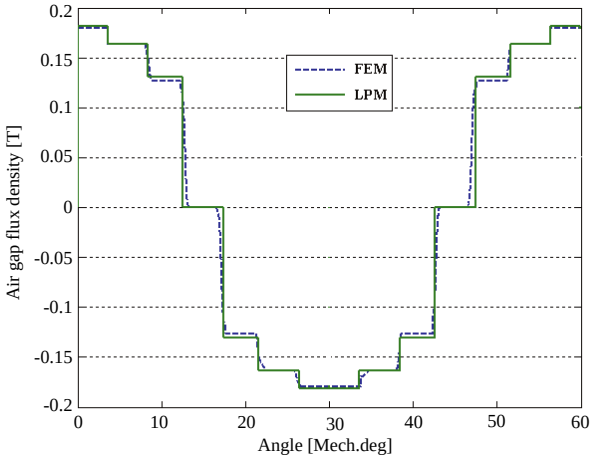

Figure 4. Air gap flux density without slot effect.

be simplified to Figure 3(b) due to symmetry. In this figure, the Kirchhoff's law is applied to loops 1–7, and nodes 1–3. So φ_{gk} for $k = 1$ to 3 can be obtained and average air-gap flux densities are $B_{g1} = \frac{\varphi_{g1}}{A_{g1}}$, $B_{g2} = \frac{\varphi_{g2}}{A_{g2}}$, $B_{g3} = \frac{\varphi_{g3}}{A_{g3}}$, respectively.

Figure 4 shows the resultant air gap flux without stator slot effects. For calculating of λ_{PM}, air gap g is substituted with $(g_e = K_c g)$ in all of equation above, where K_c is the Carter coefficient. Flux linkage calculation using LPM yields 9.2 mwb while flux calculation using FEM yields 9.3 mwb.

4. *D*-AXIS INDUCTANCE

The D-axis inductance is sum of the magnetization inductance and the leakage inductance [6].

$$L_d = L_{dm} + L_l \tag{8}$$

L_l can be calculated as described in [1]. An analytical relationship between the unsaturated Q-axis inductance and the D-axis inductance was developed by Vagati in [23]. Therefore, in this paper the d-axis inductance will be given without detailed derivation of the equations. The D-axis magnetizing inductance is composed of 'through' and 'circulating' components. As described in [6] L_{dt} and L_{dc} are estimated using magnetic circuit analysis based on formulas given in [23].

$$L_{dm} = L_{dt} + L_{dc} \tag{9}$$

Figure 5(a) shows the per-unit magnetic circuit for IPMS machine with three-layers which is solved to determine the inductance components. Several geometric quantities in Figure 5(a) need further definitions. The angle, $\Delta\alpha_k$, is defined as the angular distance at the rotor surface between adjacent magnet flux paths such that $\Delta\alpha_k = \alpha_k - \alpha_{(k-1)}$. The cross-sectional areas for the total stator air gap surface, A_r, for stator tooth pitch A_s, for each central post A_{ck}, and for each magnet A_{mk}, are defined as $A_r = 2\pi R_{si} L$, $A_s = \frac{A_r}{Q_s}$, $A_{ck} = w_c L$, and $A_{mk} = w_{mk} L$.

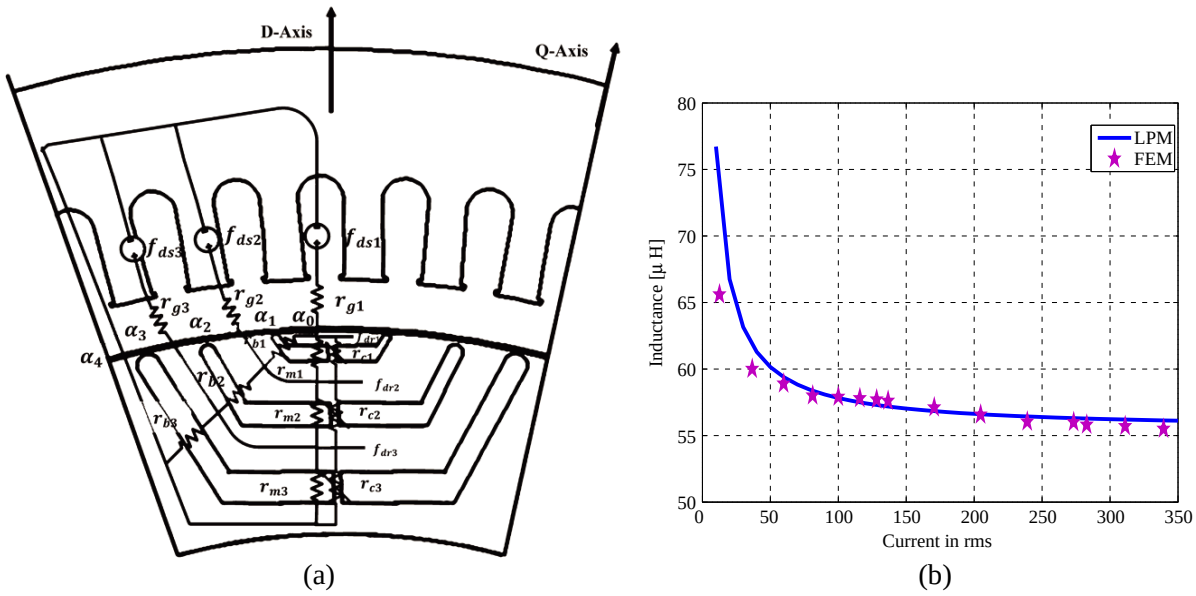

Figure 5. Equivalent circuit and inductance of d-axis. (a) Equivalent d-axis inductance LPM circuit. (b) Comparison of D-axis inductance using FEM and LPM.

Then per-unit circuit reluctance for magnet cavity and air gap segment can be defined as:

$$r_{mk} = \frac{2h_{mk}A_s}{g_e A_{mk}} \tag{10}$$

$$r_{gk} = \frac{\Delta\alpha_s}{\Delta\alpha_k} \tag{11}$$

$$r_{ck} = \frac{2h_{mk}A_s}{g_e A_{ck}} \left(\frac{I_{ds}}{I_b}\right) \tag{12}$$

r_{ck} is per-unit circuit reluctance for central post. Air bridge flux density variation with regard to changes in D-axis current is negligible. However, central post flux varies with the changes in d-axis current, therefore, $\frac{I_{ds}}{I_b}$ coefficient is considered to compensate for these variations where I_{ds} and I_b are D-axis current and base current, respectively. The stator mmf per unit source for the kth peripheral segment is expressed as [12]:

$$f_{dsk} = \frac{\cos(\alpha_{k-1}) - \cos(\alpha_k)}{\Delta\alpha_k} \tag{13}$$

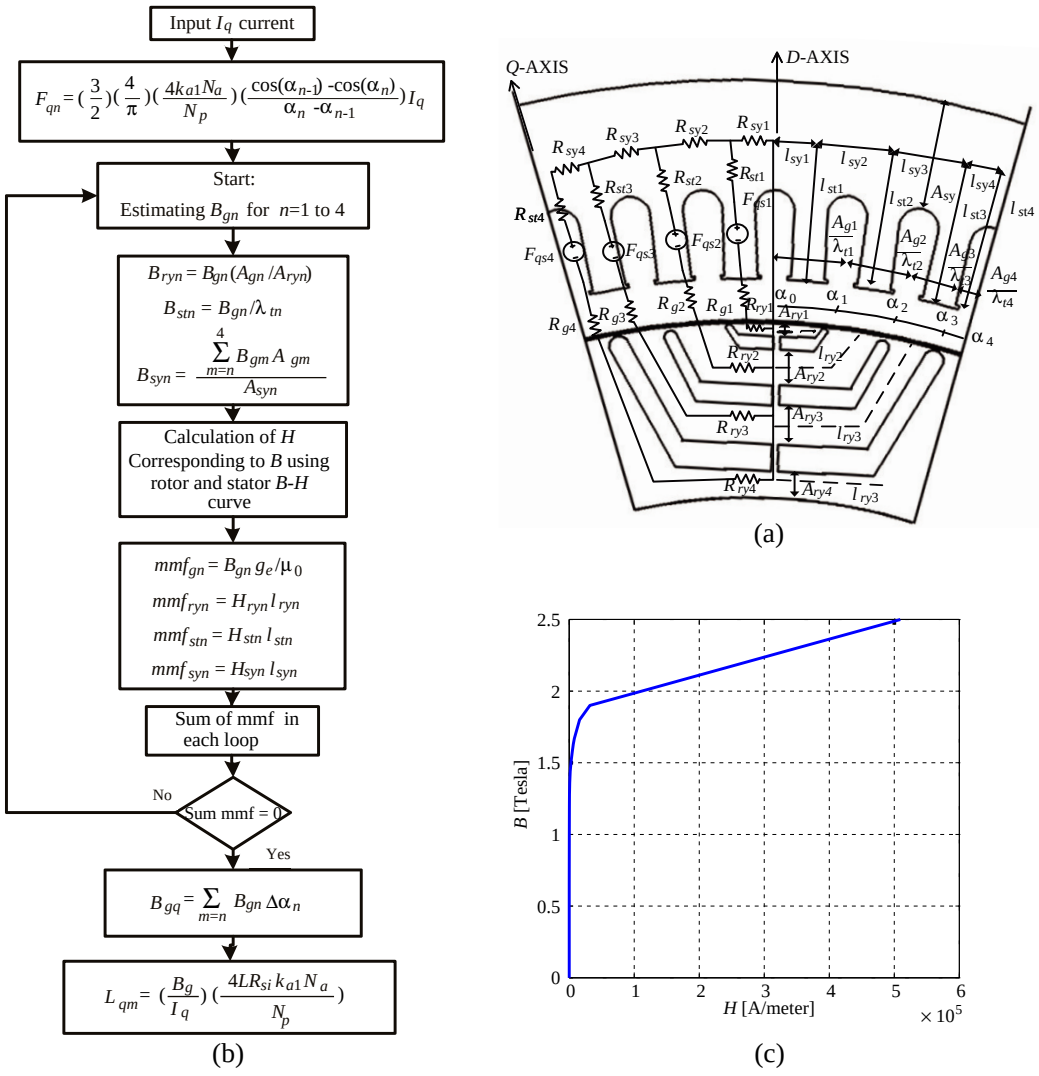

Figure 6. Calculation of Q-axis reluctance. (a) LPM for Q-axis inductances. (b) Flowchart for calculating Q-axis inductance. (c) B-H curve of M-19 steel.

For calculating f_{drk} we can use the Kirchhoff's law [3]. The D-axis inductance is calculated using the following equations [12, 23]:

$$\frac{L_{dc}}{L_{qm}} = 1 - \frac{4}{\pi}\sum_k \Delta\alpha_k f_{dsk}^2 \tag{14}$$

$$\frac{L_{dt}}{L_{qm}} = \frac{4}{\pi}\sum_k f_{dsk}(f_{dsk} - f_{drk})\Delta\alpha_k \tag{15}$$

where L_{qm} is Q-axis magnetization inductance and can be calculated from round rotor air gap inductance [1]:

$$L_{ag} = L_{qm} = \frac{3}{2}\left(\frac{4}{\pi}\right)\frac{\mu_0 N_a^2 K_{a1}^2 L R_{si}}{\left(\frac{N_p}{2}\right)^2 g_e} \tag{16}$$

The D-axis total magnetizing inductance is given by:

$$L_{dm} = \left(\frac{L_{dc}}{L_{qm}} + \frac{L_{dt}}{L_{qm}}\right) L_{qm} \tag{17}$$

Figure 5(b) shows that the variation of D-axis inductance ($L_d = L_{dm} + L_l$) versus the current for the LPM and FEM methods, which are in great agreement.

5. *Q*-AXIS INDUCTANCE

For high-performance applications, the exciting MMF is likely to drive the Q-axis path into the saturation region of the core material. To accurately predict L_q under rated load condition, a saturated model of the LPM is used here [6]. Figure 6(a) shows Q-axis reluctance model of the stator and rotor. In this model, the stator is partitioned in a manner similar to rotor. It is assumed that the magnetic flux is carried in a single flux tube from each rotor segment through the stator back iron. The element lengths are defined as the average length through each segment and are shown in Figure 6(a). In this figure, λ_{tn} is the effective teeth area that calculated using the air gap area scaled by the slot pitch fraction. The MMF drop across each reluctance is calculated instead of calculating the reluctances. For calculating L_q using this model the LPM is solved iteratively along each branch using the flowchart shown in Figure 6(b). Figure 6(c) shows B-H curve of M-19 steel for stator and rotor core.

Figure 7(a) shows the Q-axis inductances ($L_q = L_{qm} + L_l$) obtained from FEM and LPM which again shows great agreement.

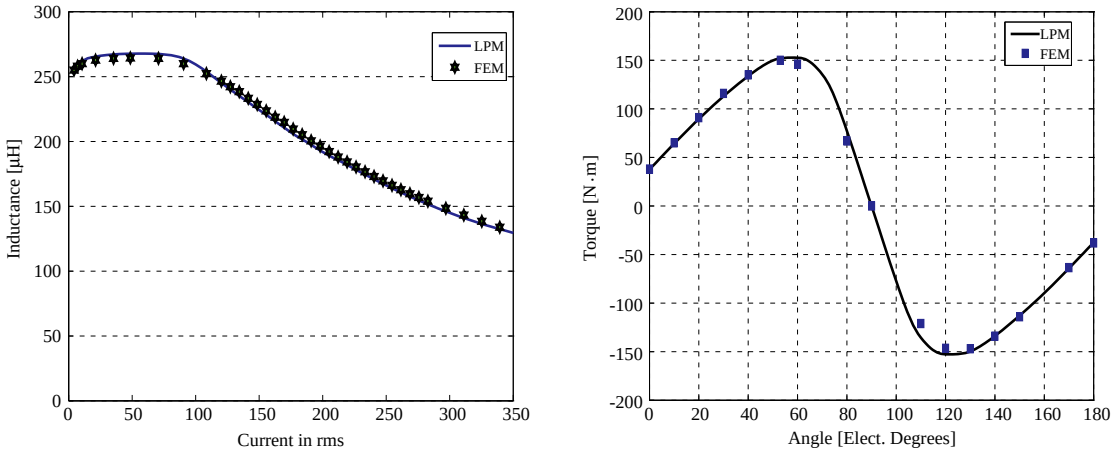

Figure 7. Comparison of Q-axis inductance and torque calculated. (a) Comparison of Q-axis inductance calculated using FEM and LPM. (b) Comparison of electromagnetic torque calculated using FEM and LPM.

6. TORQUE CALCULATION

We are interested in calculating the electromagnetic torque produced by the IPMS machine using LPM analysis. To validate the model, the results are compared with FEM results for a candidate IPMS machine. Figure 7(b) shows electromagnetic torque calculated using FEM and lumped parameter models versus torque angle with constant rms phase current, which shows the good accuracy of LPM method.

7. CONCLUSION

Comparison of the results obtained by the two methods (LPM and FEA) for inductances of D and Q-axis and electromagnetic torque shows the accuracy of the LPM method for three-layer IPMS machine having flux barrier and central posts. The improvement employed in the calculation of the D-axis inductance has resulted in more accuracy of D-axis inductance in lower currents. Because of the few number of the elements used for calculation of inductances in the proposed LPM method, it can be used as one of the most efficient methods in the design optimization process. The model is modified to include flux barriers, central posts, and saturation at heavy loading conditions.

REFERENCES

1. Miller, T. J. E., *Brushless Permanent-magnet and Reluctance Motor Drives*, 3rd Edition, Oxford University Press, 1989.
2. Boldea, I., *Reluctance Synchronous Machines and Drives*, Oxford University Press, 1996.
3. Zhu, L., S. Z. Jiang, Z. Zhu, and C. Chan, "Analytical modeling of open-circuit air-gap field distributions in multisegment and multilayer interior permanent-magnet machines," *IEEE Trans. Mag.*, Vol. 45, No. 8, 3121–3130, 2009.
4. Zhu, Z., D. Howe, E. Bolte, and B. Ackermann, "Instantaneous magnetic field distribution in brushless permanent magnet DC motors. Part I. Open-circuit field," *IEEE Trans. Mag.*, Vol. 29, No. 1, 124–135, 1993.
5. Hwanga, C., C. Changa, C. Panb, and T. Changc, "Estimation of parameters of interior permanent magnet synchronous motors," *Journal of Magnetism and Magnetic Materials*, Vol. 239, Nos. 1–3, 600–603, 2006.
6. Lovelace, E., T. Jahns, and J. H. Lang, "A saturating lumped-parameter model for an interior PM synchronous machine," *IEEE Transaction on Industry Applications*, Vol. 38, No. 3, 645–650, 2002.
7. Tariq, A., C. Nino Baron, and E. Strangas, "Iron and magnet losses and torque calculation of interior permanent magnet synchronous machines using magnetic equivalent circuit," *IEEE Trans. Mag.*, Vol. 46, No. 12, 4073–4080, 2010.
8. Amrhein, M. and P. Krein, "Induction machine modeling approach based on 3-D magnetic equivalent circuit framework," *IEEE Transactions on Energy Conversion*, Vol. 25, No. 2, 339–347, 2010.
9. Zhu, Z., Y. Pang, D. Howe, S. Iwasaki, R. Deodhar, and A. Pride, "Analysis of electromagnetic performance of flux-switching permanent-magnet Machines by nonlinear adaptive lumped parameter magnetic circuit model," *IEEE Trans. Mag.*, Vol. 41, No. 11, 4277–4287, 2005.
10. Bash, M. and S. Pekarek, "Modeling of salient-pole wound-rotor synchronous machines for population-based design," *IEEE Transaction on Energy Conversion*, Vol. 26, No. 2, 381–392, 2011.
11. Zhu, Z., D. Howe, and C. Chan, "Improved analytical model for predicting the magnetic field distribution in brushless permanent-magnet machines," *IEEE Trans. Mag.*, Vol. 38, No. 1, 229–238, 2002.
12. Lovelace, E. C. F., "Optimization of a magnetically saturable interior permanent-magnet synchronous machine drives," Ph.D. Dissertation, MIT, 2000.
13. Hwang, C. C., and Y. H. Cho, "Effects of leakage flux on magnetic fields of interior permanent magnet synchronous motors," *IEEE Trans. Mag.*, Vol. 37, No. 4, 3021–3024, 2001.

14. Rahman, M., T. Little, and G. Slemon, "Analytical models for interior-type permanent magnet synchronous motors," *IEEE Trans. Mag.*, Vol. 21, No. 5, 1741–1743, 1985.
15. Mirahki, H., M. Moallem, and S. Rahimi, "Design optimization of IPMSM for 42 V integrated starter-alternator using lumped parameter model and genetic algorithms," *IEEE Trans. Mag.*, Vol. 50, No. 3, 114–119, 2014.
16. Bracikowski, N., M. Hecquet, P. Brochet, and S. V. Shirinskii, "Multiphysics modeling of a permanent magnet synchronous machine by using lumped models," *IEEE Trans. Mag.*, Vol. 59, No. 6, 2426–2437, 2012.
17. Zhu, Z., D. Howe, and Z. Xia, "Prediction of open-circuit airgap field distribution in brushless machines having an inset permanent magnet rotor topology," *IEEE Trans. Mag.*, Vol. 30, No. 1, 98–107, 1994.
18. Wang, J., D. Lieu, W. Lorimer, and A. Hartman, "Comparison of lumped parameter and finite element magnetic modeling in a brushless DC motor," *IEEE Trans. Mag.*, Vol. 33, No. 5, 4092–4094, 1997.
19. Hsieh, M. F. and Y. C. Hsu, "A generalized magnetic circuit modeling approach for design of surface permanent-magnet machines," *IEEE Transactions on Industrial Electronics*, Vol. 59, No. 2, 779–792, 2012.
20. Mi, C., M. Filippa, W. Liu, and R. Ma, "Analytical method for predicting the air-gap flux of interior-type permanent-magnet machines," *IEEE Transactions on Industrial Electronics*, Vol. 40, No. 1, 50–58, 2004.
21. Vagati, A., M. Pastorelli, F. Scapino, and G. Franceschini, "Effect of magnetic cross-coupling in synchronous reluctance motors," *Intelligent Motion Conference*, Vol. 1, 279–285, 1997.
22. Vagati, A., M. Pastorelli, F. Scapino, and G. Franceschini, "Cross-saturation in synchronous reluctance motors of the transverse-laminated type," *Industry Applications Conference, Thirty-Third IAS Annual Meeting*, Vol. 1, 127–135, 1998.
23. Vagati, A., M. Pastorelli, F. Scapino, and G. Franceschini, "Design criteria of an IPM machine suitable for field-weakened operation," *International Conference on Electrical Machine*, 1059–1065, 1999.